CAV2021
11th International Symposium on Cavitation
May 10-13, 2021, Daejon, Korea

Experimental Investigation of Cavitation in a Jet Regarding Process Optimization

Julius-Alexander Nöpel *, Jochen Fröhlich and Frank Rüdiger

Institute of Fluid Mechanics, TU Dresden, Germany

Abstract: This study of a cavitating jet in a reactor with different nozzle diameters and pressure differences is focused on evaluating a cavitation flow in terms of process engineering use, for process optimization and for reproducibility of the experiment. For this purpose, optical images of the flow were acquired, significant process variables were measured and compared with degradation of the dye Congo red and chemiluminescence of luminol. It was found, that within the range of parameter variation in the presented study, the ratio of degradation and energy consumption is tending to be optimal for small nozzles. A correlation has been found between the ratio of degradation and the oxygen saturation in the equilibrium state of the process. As an important fact for increasing degradation the stability of the cavitation due to the absence of large scale vortices in the initial section of the jet has been identified.

Keywords: Hydrodynamic cavitation, degradation, optical measurement, energy efficiency

1. Introduction

Advanced oxidation processes (AOP) based on the application of hydrodynamic cavitation have been investigated for degradation of diverse substances using various devices [1, 2]. One of the main problems for application of this technology is the high energy consumption. Optimization is restricted by the unknown local conditions in the flow field with cavitation. To reproduce and optimize a cavitation process, a variety of relevant parameters, such as pressure, temperature, pH-value, conductivity, redox potential and oxygen saturation, have to be measured. In addition to these process factors, the most important object in cavitation is the analysis of bubble formation and collapse. Furthermore, estimation of the potential in oxidative degradation is required, which can be obtained by a known method of evidence [3].

The present study presents progress to close this gap and provides a basis for process evaluation and optimization for AOP using cavitation devices with a jet. The dye Congo red and chemiluminescence of luminol together with optical methods are used to investigate degradation, the local flow and cavitation region in the reactor. The following theses for cavitation in a jet are postulated: (I) AOP is more energy efficient for smaller nozzle size. (II) Outgassing increases with smaller nozzle diameter and correlates to degradation. (III) Stability of cavitating jet stimulates degradation.

2. Materials and Methods

The experimental setup shown in Figure 1a, consists of a stainless steel pipe system, a Piston diaphragm pump (HydraCell G10X, Verder, Germany), an open stainless steel tank and a reactor. The reactor has a volume of $V_R = 22.5$ cm^3 with a cross-sectional area of 15 x 15 mm^2. A single, exchangeable nozzle is located in the center of the reactor. Nozzle diameters of $d = \{0.6; 1; 1.7\}$ mm are used and pressure differences of up to $\Delta p = 30$ bar are generated. The setup contains two liters of water, the fluid temperature was permanently kept in the range of $T = (30 \pm 5)$ °C by a cooling unit (Hydac, Germany).

Pressure is measured upstream (p_1) and downstream (p_2) the reactor. The pressure difference Δp is defined by $\Delta p = p_1 - p_2$. The values of pH, conductivity σ, oxygen saturation sO_2, redox potential E^0 and temperature T were continuously measured in the tank.

* Corresponding Author: Julius-A. Nöpel, Julius-Alexander.Noepel@tu-dresden.de

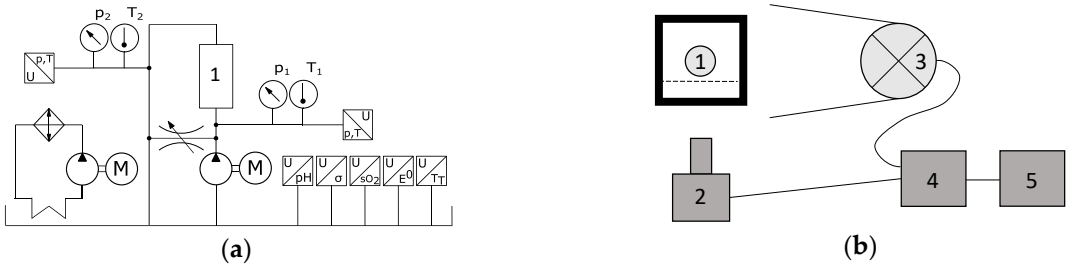

(**a**) (**b**)

Figure 1. Setup of the experimental configuration and the optical acquisition system. (a): Hydraulic circuit of the experimental setup; (b): Position of the measuring equipment for optical imaging: 1 – reactor, 2 – high-speed camera, 3 - high performance light emitter, 4 – synchronizer, 5 – computer. Dashed line indicates image plane.

For optical accessibility, the reactor has acrylic glass walls. The setup for image acquisition is sketched in Figure 1b. For the visualization of the oxidative species, $V = 2$ l of an alkaline *luminol* solution ($c = 2.0$ g/l of luminol (CAS: 521-31-3, 98% purity from Alfa Aesar), $c = 5.0$ g/l of Na_2CO_3, dissolved in deionized water) was filled into the system circuit. The chemiluminescence was recorded with the SLR camera (Canon EOS 650D, EF 50 mm 1:1,8 STM) at an exposure time of $t_e = 300$ s. The distance between the reactor and the camera sensor was $l_c = 410$ mm. All images were processed equally as described in [4].

For the dye degradation experiments, a solution of *Congo red* (CAS: 573-58-0, from Alfa Aesar) with a concentration of $c_0 = 30$ mg/l is filled into the system. Because of the filling of the system and possible concentration changes, the pump has been operated for several system volume passes, without cavitation in the reactor. Then the first sample was taken to determine the initial concentration and the treatment procedure has been started. Long-term tests without cavitation did show no further degradation. The samples were analyzed by spectrophotometry.

3. Results

3.1. Fluid mechanical properties and reactivity of the cavitating jet

In the follwing, three different configurations are discussed in detail: 0630, 1030 and 1730. The configurations are identified according to a uniform naming convention: for example, the configuration 0630 refers to the use of a nozzle with a diameter of $d = 0.6$ mm at a pressure difference of $\Delta p = 30$ bar. All experiments were done at least twice for reproducibility.

Figure 2 shows images for each configuration at an exposure time of $t_e = 20$ ms, which can be interpreted as a time-averaged shape of the bubble region. In addition high temporal resolution images obtained with high-speed camera at $t_e = 11$ µs and the chemiluminescence of luminol are shown, which marks the reaction area with the emission of blue light. The cavitation number Ka, with $Ka = (p_\infty - p_v)/\Delta p$, is the same for all configurations, whereas the Reynolds number Re, with $Re = w_d\, d/\boldsymbol{\nu}$, increases due to the change in nozzle diameter. The values of the two dimensionless numbers, as well as P, the hydraulic power input into the system, are given in Figure 2.

In the high temporal resolution images in Figure 2, taken by a high-speed camera (HSC), the different extension of the bubble area and the associated increasing number of bubbles with increasing nozzle diameter of the shedding of cavitation clouds are clearly visible. The jet length in the instantaneous images almost doubles from 0630 to 1730. For 0630 the jet or bubble area appears narrow and short. Moreover, the region where the bubbles collapse can be well defined.

* Corresponding Author: Julius-A. Nöpel, Julius-Alexander.Noepel@tu-dresden.de

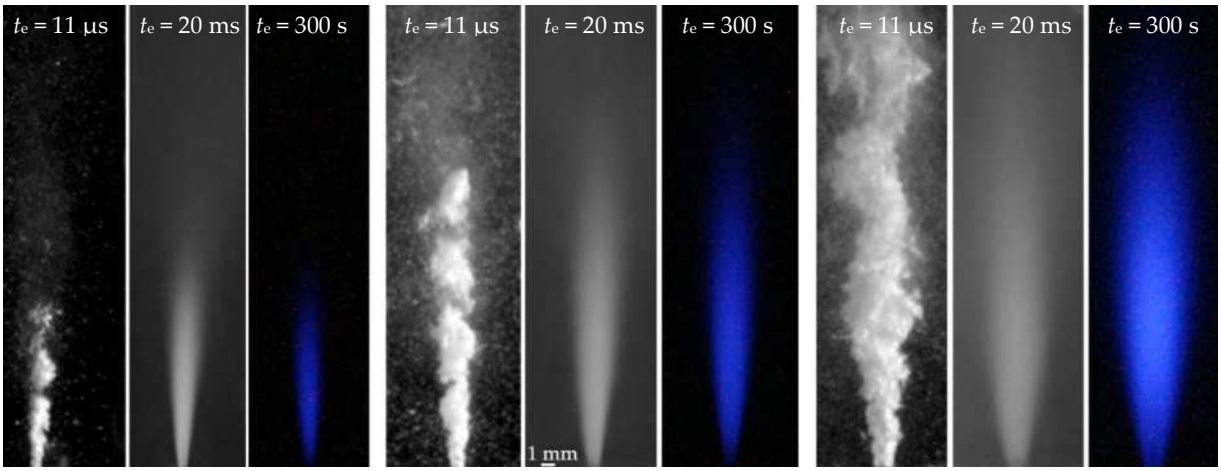

0630	**1030**	**1730**
Re = 29,700; *Ka* = 0.03; *P* = 54 W	*Re* = 52,000; *Ka* = 0.03; *P* = 124 W	*Re* = 85,400; *Ka* = 0.03; *P* = 350 W

Figure 2. Images of the cavitating jet in the reactor for three different nozzle diameters d operating at the same pressure difference Δp. For each configuration, three images are displayed in the following order: Left - image recorded with high-speed camera and high-power light source at t_e = 11 µs; Middle - image acquired with SLR camera at t_e = 20 ms; Right - long exposure image of chemiluminescence by luminol obtained with SLR camera at t_e = 300 s. Specification of Reynolds number $Re = w_d\, d/\nu$, cavitation number $Ka = (p_\infty - p_v)/\Delta p$ and hydraulic power $P = \Delta p V/t$.

In the time-averaged images in Figure 2 it can be observed, that the jet opening angle and width of the jet increases with the nozzle diameter. At 1730, the jet opening angle is significantly larger, which is due to the higher volume flow rate and bubble density, as well as the higher Reynolds number. For the same cavitation number, an extremely different extent of area affected by cavitation is evident. Finally, it should be mentioned that the smaller the pressure ratio, the fewer bubbles are present. The measured process variables were at T = 30 °C ± 5 °C, the water quality corresponded to deionized saturated water with a conductivity of σ = 20 µS/cm. The pH value was pH = 7.8 ± 0.2.

After collapse, outgassed air bubbles are present. In principle, the distance between the jet and the reactor wall is largest at 0630, resulting in low intensive secondary flow with large rate of bubble coalescence. At 1730, the bubble density in the reactor is high, the collapse region is widely extended and can no longer be clearly determined. In addition, many bubbles are in recirculation, the secondary flow velocity is larger. The spatial limitation of the expansion of the jet can be observed at 1730 on the basis of the bubble area.

In Figure 2, also the areas of chemiluminescence are shown. An increase similar to the bubble area can be observed. The increase in bubble density affects the light scattering of the blue light emitted in the jet as well as the stronger refraction of light at high bubble density leads to an enlargement of the luminous area. However, chemiluminescence of luminol can bring evidence to the presence of oxidation as a degradation effect. The pH value in the experiments was pH = 9, which was due to the luminol solution.

3.2. Effects of oxygen saturation and turbulence

Due to strong bubble formation and associated outgassing process of air, oxygen saturation in water changes during treatment time. Figure 3a shows the change in oxygen saturation over time for the three configurations introduced in Figure 2.

* Corresponding Author: Julius-A. Nöpel, Julius-Alexander.Noepel@tu-dresden.de

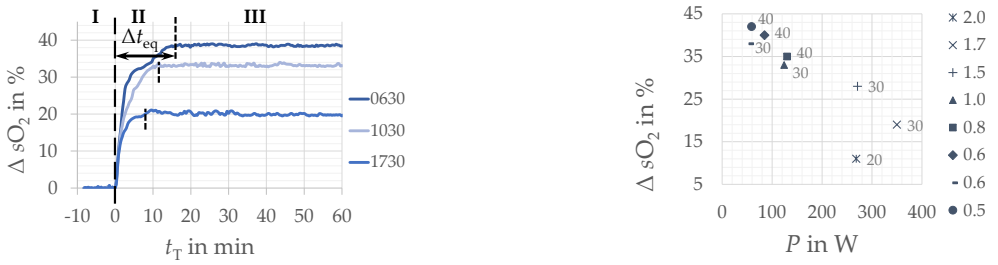

(**a**) (**b**)

Figure 3. Characteristics of the cavitating flow in the reactor: (a) Oxygen saturation change in the system with cavitating jet plotted over treatment time for configurations 0630, 1030 and 1730. Marking three sections of saturation change: I - Initial equilibrium state, II - adaption phase of time Δt_{eq} and III - new rebalanced equilibrium state in active cavitation process. (b) Change of oxygen saturation after reaching the equilibrium state in the process with cavitation for different nozzle and pressure difference configurations over hydraulic power

For the process, three sections can be identified. In section (I), an initial state of equilibrium without a cavitating free jet prevails. In section (II), the oxygen saturation adjusts in a configuration-dependent period of time Δt_{eq}. Section (III) reflects the rebalanced equilibrium in the active cavitation process. It is noted that for 0630 the duration Δt_{eq} is the largest and reduction of oxygen saturation the highest. Figure 3b shows the saturation level of the rebalanced equilibrium (Section III) for nozzle diameters from $d = 0.5$ mm to $d = 2$ mm plotted against hydraulic power P. Starting from 0630, the strength of the outgassing process falls as the nozzle diameter increases and the power rises.

On images in Figure 2, a different jet formation at the same pressure ratio is clearly visible on the basis of the bubble region. This is related to the different Reynolds number and a changed turbulence of the jet.

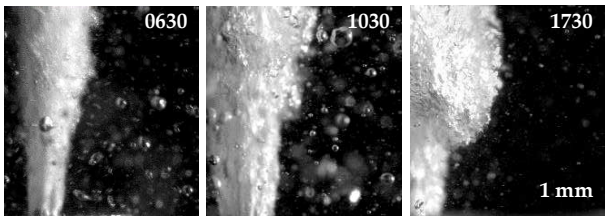

Figure 4. Microscopic images of the jet from nozzle exit entering the reactor chamber with a frame rate of $f = 71$ kHz for nozzle diameter $d = 0.6$, 1.0 and 1.7 mm (from left to right) at pressure difference of $\Delta p = 30$ bar.

Microscopic images with an exposure time of $t_e = 3$ µs are shown in Figure 4. For 0630, the jet cavitation is smooth and stable after the nozzle exit, but a transitional state can be observed, leading to the formation of vortex structures at a distance of $2d$ from the nozzle. In 1030, a smooth region is only visible just behind the nozzle exit. At a distance of $2d$ from the nozzle large-scale vortex structures are visible. In 1730 formation of large turbulent vortex structures starts shortly after the nozzle. The Reynolds number for 1730 is higher by a factor of 3 compared to 0630.

3.3. Degradation and process data

The degradation of the dye Congo red serves as a reference substance for estimating the degradation performance. Figure 5 shows the degradation of Congo red in percent via the process-related change in oxygen saturation (Section III) at a constant number of passes through the system at an input energy of $E = 0.35$ MJ for different configurations. The initial process values were the same for the degradation study before starting treatment with cavitation. It can be observed that the highest degradation occurs in configuration 0640. Globally, the degradation in other configurations decreases with the nozzle diameter at a similar pressure ratio. Thereby, the change in oxygen saturation increases with the degradation. Small

* Corresponding Author: Julius-A. Nöpel, Julius-Alexander.Noepel@tu-dresden.de

nozzles such as 0640 are energetically the most efficient, as it requires only 24 % of the power of 1730, while achieving three times the degradation. In terms of time, the treatment time t_T of 0640 is a factor of 5 higher than 1730, which can be seen in Figure 5 for the time of treatment for each configuration.

In experiments with configuration $d = 0.6$ mm and significantly higher pressure differences up to $\Delta p = 160$ bar, a reduction in degradation with increasing pressure differences was observed. The number of bubbles present in the reactor increases to values comparable to those in 1730, along with the Reynolds number.

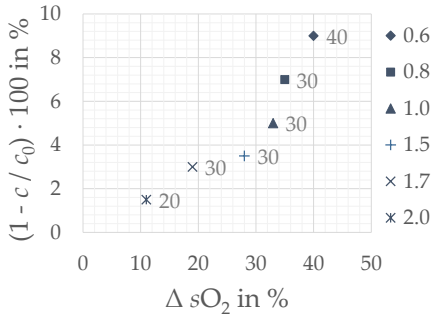

Configuration	t_T in min
0640	70
0830	45
1030	35
1530	16
1730	13
2020	11

Figure 5. Treatment of dye Congo red by cavitation: Degradation ratio of Congo red in percent over decrease of oxygen saturation in percent by processing with cavitation for various nozzle and pressure difference configurations at constant number of system volume passes $N_{svp} = 35$ and equal input of hydraulic energy $E = 0.35$ MJ. Treatment time in minutes for each configuration.

4. Conclusions

In the experimental investigation, it was found that configuration 0640 revealed the best ratio of degradation to energy input. Thereby, a strong and relatively fast reduction of the oxygen saturation by $\Delta sO_2 = 40$ % occurred in the system at 0640. The condition of the flow was characterized by a relatively low concentration of bubbles collapsing in a small definable region in the reactor compared to 1730. Changes in turbulence were observable in the initial zone of the jet, shortly after nozzle exit. The treatment of chemical substances by cavitating flows are primarily characterized by the bubble properties, which have a direct dependence on the formation of reactive species.

Acknowledgments: This work was supported by the federal ministry for economic affairs and energy (BMWi) by a resolution of the German Bundestag (16KN073422).

References

1. Braeutigam, P. et al. Degradation of carbamazepine in environmentally relevant concentrations in water by Hydrodynamic-Acoustic-Cavitation (HAC). Water Research, 2012, 46, pp. 2469-2477.
2. Saharan, V.K. et al. Effect of geometry of hydrodynamically cavitating device on degradation of orange-G. Ultrason. Sonochem., 2013, 20, pp. 345-353.
3. Arrojo, S.; Nerin, C.; Benito, Y. Application of salicylic acid dosimetry to evaluate hydrodynamic cavitation as an advanced oxidation process. Ultrason. Sonochem., 2007, 13, pp. 343-349.
4. Nöpel, J.-A. et al. Experimental investigation of the bubble distribution and chemical reactions induced by hydrodynamic cavitation inside a reactor-a preliminary study. Conference Proceedings 5th ICEFM, Munich, Germany, 2018, pp. 679–684.

* Corresponding Author: Julius-A. Nöpel, Julius-Alexander.Noepel@tu-dresden.de